CHEMISTRY
A EUROPEAN JOURNAL

DOI: 10.1002/chem.200700254

Towards a Rational Design of Ruthenium CO_2 Hydrogenation Catalysts by Ab Initio Metadynamics

Atsushi Urakawa,[a] Marcella Iannuzzi,[b] Jürg Hutter,[b] and Alfons Baiker*[a]

Abstract: Complete reaction pathways relevant to CO_2 hydrogenation by using a homogeneous ruthenium dihydride catalyst ($[Ru(dmpe)_2H_2]$, dmpe = $Me_2PCH_2CH_2PMe_2$) have been investigated by ab initio metadynamics. This approach has allowed reaction intermediates to be identified and free-energy profiles to be calculated, which provide new insights into the experimentally observed reaction pathway. Our simulations indicate that CO_2 insertion, which leads to the formation of formate complexes, proceeds by a concerted insertion mechanism. It is a rapid and direct process with a relatively low activation barrier, which is in agreement with experimental observations. Subsequent H_2 insertion into the formate–Ru complex, which leads to the formation of formic acid, instead occurs via an intermediate $[Ru(\eta^2\text{-}H_2)]$ complex in which the molecular hydrogen coordinates to the ruthenium center and interacts weakly with the formate group. This step has been identified as the rate-limiting step. The reaction completes by hydrogen transfer from the $[Ru(\eta^2\text{-}H_2)]$ complex to the formate oxygen atom, which forms a dihydrogen-bonded Ru–H···HO(CHO) complex. The activation energy for the H_2 insertion step is lower for the *trans* isomer than for the *cis* isomer. A simple measure of the catalytic activity was proposed based on the structure of the transition state of the identified rate-limiting step. From this measure, the relationship between catalysts with different ligands and their experimental catalytic activities can be explained.

Keywords: carbon dioxide fixation · density functional calculations · hydrogenation · molecular dynamics · ruthenium

Introduction

The utilization of CO_2 as a possible carbon source and as a medium for reaction and extraction processes has been increasingly investigated.[1,2] This increased attention has been triggered by ever-growing environmental concerns[3,4] and the scientific challenge to activate this rather inert molecule.[5–8] In the 1990s, several reactions based on CO_2 hydrogenation were reported in which CO_2 was used both as a solvent and as a reactant under supercritical conditions.[9–14] Formic acid, alkyl formates, and formamides have been successfully synthesized with high turnover frequencies. In particular, the high activity of the ruthenium catalysts used offers the possibility of utilizing CO_2 as a C_1 building block through its hydrogenation. The formation of formic acid by CO_2 hydrogenation has been identified as the first reaction step in the three different reaction systems mentioned above.[12] Hence, elucidation of the pathways for formic acid formation is necessary to understand several aspects of the reaction process, such as the detailed reaction mechanisms, the effects of different ligands,[12,15] the role of additives (water, alcohols, and amines),[12,16,17] and the influence of reactant pressure.[12,16,18] Detailed reaction mechanisms have been proposed to date, but discrepancies between the mechanisms and experimental observations exist,[19,20] such as the discrepancy between the theoretical assignment of CO_2 insertion into a ruthenium hydride complex as the rate-limiting step and the experimentally observed facile CO_2 insertion.[21,22] A confident assignment of the rate-limiting step and understanding of the nature of the corresponding transition state is still lacking for rational catalyst design.

The goal of this work was to shed light on the competitive reaction pathways leading to CO_2 hydrogenation by a single-site homogeneous ruthenium catalyst. This study was mainly based on ab initio molecular dynamics with the help of complementary experimental work.[21] To simplify the in-

[a] Dr. A. Urakawa, Prof. Dr. A. Baiker
Institute for Chemical and Bioengineering
Department of Chemistry and Applied Biosciences
ETH Zurich, Hönggerberg, HCI
8093 Zurich (Switzerland)
Fax: (+41) 44-632-1163
E-mail: baiker@chem.ethz.ch

[b] Dr. M. Iannuzzi, Prof. Dr. J. Hutter
Physical Chemistry Institute, University of Zurich
Winterthurerstrasse 190, 8057 Zurich (Switzerland)

terpretation of the experimental spectra, a dihydride catalyst with a bridged ligand, dmpe (dmpe = $Me_2PCH_2CH_2PMe_2$), was chosen because of its structural rigidity and its activity in the reaction.[12,13] The complex is also suitable for computational modeling, thanks to its relatively small size.

The synthesis and structure of the ruthenium dihydride catalyst [Ru(dmpe)$_2$H$_2$] have been reported in a previous paper.[21] High-pressure spectroscopy measurements (IR and NMR) carried out in toluene at 300 K have been used to study the transformations of the catalyst that were induced by different concentrations of CO_2, H_2, and formic acid. In Scheme 1, two possible sequences of intermediates are proposed on the basis of experimental results. The measurements show that the *cis* isomer **1** of the dihydride catalyst is predominant (94.5%) over the *trans* isomer **4** (5.5%). Under low CO_2 pressure (<5 bar), two formate complexes appear, *cis*-[Ru(dmpe)$_2$(OCHO)$_2$] (**3**) and *trans*-[Ru(dmpe)$_2$H(OCHO)] (**5**). No evidence for the expected *cis*-[Ru(dmpe)$_2$H(OCHO)] complex (**2**) has been revealed, even if this structure should be the natural intermediate between **1** and **3**. Indeed, at 300 K complex **2** is a short-lived structure owing to its lower stability relative to **3**, which explains why it has not been observed.[22] When an additional high H_2 pressure (>50 bar) was applied, the signal of the dihydrogen-bonded complex *trans*-[Ru(dmpe)$_2$H$_2$]···HOCHO (**6**) was also detected and its intensity increased with H_2 pressure.[21]

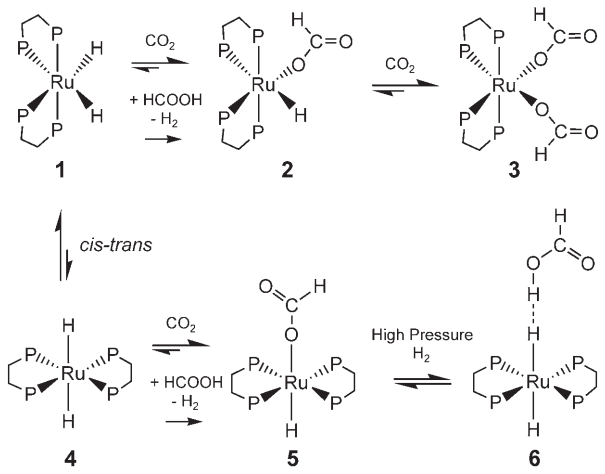

Scheme 1. The main ruthenium complexes observed in toluene at 300 K in the presence of CO_2 and H_2. Note that complex **2** has been observed at 223 K,[22] but not at 300 K.[21]

To verify the proposed pathways and to identify the rate-limiting step, we needed to investigate the relevant reaction intermediates and transition states in more detail. Density functional theory (DFT) calculations have been proven to be able to reproduce the relative energies of the different stable complexes, and are in agreement with experimental findings.[21] Starting from reasonable guesses based on experimental observations and by optimizing the structures of minimum energy conformers or transition states, it was possible to suggest an approximate sequence of steps along the reaction mechanism. However, this static approach is likely to fail for complex processes in which several alternative routes are possible and unforeseen intermediate states may play an important role. In addition, finite temperature effects and entropic contributions cannot be included in a static model.

To gain a complete picture of the process and to determine the rate-limiting step and the most probable route, a better understanding of the atomistic details of CO_2 and H_2 insertions is necessary. The relative probability of competitive events like *cis*/*trans* isomerization and CO_2 dissociation should also be taken into account.

A complete description of the reaction routes and discrimination between competitive pathways can be provided by molecular dynamics (MD). The technique is, in principle, capable of generating reactive trajectories. The kinetics of the process can be investigated and from statistical sampling the underlying free-energy surface (FES) can be reconstructed. The evolution of the electronic structure associated with the structural rearrangements is also accessible from ab initio MD, thus offering a deeper insight into the chemistry of the transformation events. However, for adequate sampling by standard MD, a great amount of simulation time is typically required, which frustrates its predictive capability at all levels of theory. We have chosen, therefore, to adopt the metadynamics (MTD) approach to boost the sampling.[23,24] This method has been successfully applied in combination with ab initio MD to the study of various types of reactive systems in which substantial changes to the electronic structure were expected.[24–31] The accuracy of the methods for the calculation of the FES has been verified[32] by comparison with other techniques.[33–35]

Ab initio metadynamics: Metadynamics is a method based on MD simulations that allows thorough sampling of a predefined multidimensional configurational space and provides, at the same time, the direct reconstruction of the explored FES.[23] The subspace for which we wish to boost the sampling is defined by selecting a set of collective variables (CVs) that clearly identify specific states of the system under investigation. They typically correspond to those slow modes that might play a role in the transformation of the system, and therefore, need to be activated. A rather general rule prescribes that the selected CVs are able to distinguish the relevant intermediates and competitive reactive pathways. The dynamics in the space of the CVs, that is, the metadynamics, are accelerated by the presence of a history-dependent, repulsive potential. This potential is built up "on-the-fly" during the evolution of the meta-trajectory. It locally modifies the energy profile of those regions in the configurational space that have already been visited, and thereby, prevents the trajectory from remaining in the same basin of attraction for very long time.[36] This approach enforces the exploration of the FES and enables the most probable pathways of a reaction to be disclosed, even if

there is no prior knowledge of the transition or of the products. The scope of the applications is significantly broadened by its implementation within ab initio methods,[24] such as DFT-based Car–Parrinello MD.[37] Within this scheme, it is now possible to efficiently simulate the dynamics of chemical reactions when important changes in the electronic structure take place (e.g., bond formation/breaking). MTD has been successfully applied in various fields, such as molecular biology,[38–41] catalysis,[27] phase transitions,[25,28,30,42] molecular rearrangements,[24,26] surface reactions,[31] and the structural analysis of condensed matter.[29]

The meta-trajectory is determined by integrating the equations of motion derived from an extended Lagrangian[24] of the form given by Equation (1):

$$\mathcal{L} = \mathcal{L}_{CP} + \sum_{\alpha} \frac{1}{2} M_{\alpha} \dot{s}_{\alpha}^2 - \sum_{\alpha} \frac{1}{2} k_{\alpha} [S_{\alpha}(\mathbf{R}) - s_{\alpha}]^2 + V(t,\mathbf{s}) \quad (1)$$

in which the additional dynamic variables s_α define the dynamics in the reduced space of the CV. The first term $\mathcal{L}_{CP}$ is the Car–Parrinello Lagrangian,[37] which drives the electronic and ionic dynamics. The second is the fictitious energy of the new dynamic variables. The third term is a harmonic restraint potential that couples the meta-trajectory to the standard MD trajectory through the instantaneous values of the CVs, $S_\alpha(\mathbf{R})$. The fictitious mass M_α and the coupling constant k_α determine the frequency of the fluctuations of the meta-trajectory. The last term $V(t,\mathbf{s})$ ($\boldsymbol{s}$ is the vector of s_α) is the history-dependent potential,[24] which is constructed by the accumulation of small Gaussian hills deposited at regular time intervals. At convergence, that is, when the available wells have been completely filled by the accumulated potential, the explored FES can be reconstructed from $V(t,\boldsymbol{s})$.[24]

Next in this paper we provide additional information about the methodology and the specific setup of the simulations. Then we describe the most important steps in the reaction pathways, as determined by ab initio MTD. The existence of alternative routes, different from that shown in Scheme 1, is also discussed. Finally, we provide a detailed analysis of the rate-limiting step by discussing how the catalytic activity can be associated with the electronic structure of the corresponding transition state. The same arguments can be applied to several catalysts with different ligands, showing a clear relationship between catalytic activity and electronic structure that can help in suggesting new routes for the design of efficient catalysts.

Computational Details

Ab initio MTD simulations were performed by using the Car–Parrinello (CP) scheme,[37] as implemented in the CPMD code.[24,43] Our studies were based on DFT electronic structure calculations by using plane-waves basis sets for the expansion of the wavefunctions and the pseudopotential approximation for the treatment of the ionic cores. The exchange and correlation energy terms were described by the Becke–Perdew (BP) functional.[44,45] Norm-conserving Troullier–Martins pseudopotentials were used to describe the interaction between the valence electrons and the ionic cores.[46] The energy cutoff for the plane-waves expansion was set to 80 Ry within a cubic supercell of 15 Å length. The Hartree potential was computed by the Martina–Tuckerman scheme to mimic the conditions of an isolated system in the gas phase.[47] The temperature was maintained at about 300 K by rescaling the atomic velocities. An electronic fictitious mass of 400 a.u. and a time step of 4 a.u. (0.097 fs) were used.

The first and probably most critical step in the setting up of the MTD simulations is the selection of proper CVs. In the study of chemical reactions, the natural choices are bond lengths, bond angles, dihedral angles, and coordination numbers. As already mentioned, the essential requirement is that the CVs can distinguish the different states along the entire mechanism. In this study, we made considerable use of the coordination number (CN), which is defined by the smooth function given by Equation (2):

$$CN_{AB} = \frac{1}{N_A} \sum_{i=1}^{N_A} \left[\sum_{j=1}^{N_B} \frac{1-\left(\frac{r_{ij}}{R_{AB}}\right)^p}{1-\left(\frac{r_{ij}}{R_{AB}}\right)^q} \right] \quad (2)$$

This function evaluates the average number of neighbors of type B surrounding atoms of type A within a region defined by the reference distance R_{AB}. N_A and N_B are the numbers of atoms of the two types, r_{ij} is the interatomic distance between the specific pair, and p and q determine the decay, in which $p<q$. The two exponents can be tuned to design a function as sensitive as possible to the different molecular states.

Figure 1 shows the CN functions used in this work. For example, the function in Figure 1 shown by the dotted line represents the CN between the ruthenium and oxygen atoms during the CO_2 insertion/dissociation processes. When the oxygen atom coordinates to the ruthenium center, the value of this function fluctuates between 0.5 and 1.0, whereas it is about 0.1 when the oxygen atom is too far away to be in the coordination shell of the metal. The coordination numbers can be rather general variables because, by definition, they can involve heterogeneous sets of atoms and describe the probability of there being neighboring atoms within given coordination shells. In this sense, employing coordination numbers in place of bond lengths and angles can significantly reduce the bias on the specific atomic movements.

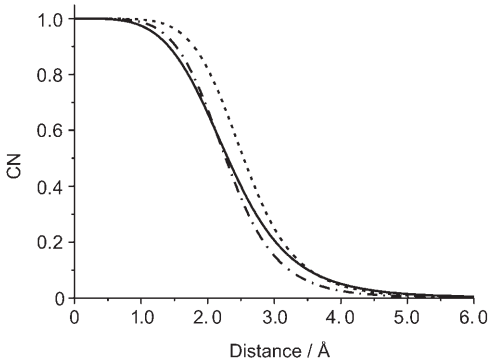

Figure 1. Coordination number (CN) functions used in this work: $p=4$, $q=6$, and $R_{AB}=2.5$ (——); $p=5$, $q=7$, and $R_{AB}=2.4$ (–•–•); and $p=6$, $q=7$, $R_{AB}=2.6$ (•••••).

A new hill was added at every so-called MTD step, which corresponds to 60 to 120 MD steps. This time interval is thought to allow a partial relaxation of the system to guarantee that the MTD trajectory follows the minimum energy pathway. In all of the reported simulations, the height of the hill was between 0.31 and 1.26 kcal mol^{-1}. The MTD drives the system towards nonequilibrium configurations and can induce fast or

abrupt rearrangements of the atomic positions. The propagation of the electronic structure through the CP scheme may not be able to adapt quickly enough, therefore, regular quenching of the wavefunctions on the Born–Oppenheimer surface at certain intervals is necessary to keep the kinetic energy of the electrons under control.

Geometry optimization, single-point energy, and harmonic vibrational frequency were also calculated to compare the electronic structures of various ruthenium complexes with different ligands. For these analyses, the B3PW91 hybrid functional[48,49] was used within the Gaussian 03 program package.[50] Although we did not see notable differences in the energy profiles and geometries of various ruthenium complexes calculated by the BP and the B3PW91 functionals, the hybrid functional was chosen for these static calculations as a result of our previous static DFT/high-pressure spectroscopic study in which the accuracy of the functional was validated by the firm assignments of various vibrational modes observed in the experimental IR spectra.[21] A 6-311G(d,p) basis set was applied to all the species except ruthenium for which a LanL2DZ effective core potential (ECP) basis set was used. The ECP replaces the core electrons of ruthenium up to 3d and the valence electrons are described by a (341/321/31) basis set. All the calculations were performed within a gas-phase model without taking any solvent effects into account.

Results and Discussion

The entire reaction process can be separated into three fundamental steps: *cis*/*trans* isomerization, CO_2 insertion, and H_2 insertion. In our investigation, we assumed that the three steps were independent processes and performed separate MTD simulations for each of them, starting from different initial configurations. By combining the results of the independent calculations, we can reconstruct several possible pathways and give an estimate of their relative probability.

***cis*/*trans* Isomerization**: Although the $[Ru(dmpe)_2H_2]$ complex is known to exist preferentially as the *cis* isomer at room temperature, by increasing the CO_2 and H_2 pressures, and thus inducing insertion processes, the signal of the *trans* isomer intensified and even became predominant. This prompted us to study how the *cis*/*trans* isomerization occurs, at which step of the overall reaction it is favored, and finally the rate at which equilibrium is attained.[51] Indeed, by considering the isomerization process at different stages, alternative transformation routes, in addition to the most obvious ones, become possible. For example, formic acid can be formed through the sequence **1**→**2**→**5**→**6**, or even through the *cis*/*trans* isomerization of the diformate complex **3**, followed by CO_2 dissociation, in addition to the expected pathway **1**→**4**→**5**→**6**. For this reason we investigated three isomerization mechanisms in detail: The dihydride isomerization (**1**⇄**4**, Scheme 1), the monoformate isomerization (**2**⇄**5**), and the diformate isomerization (**3**⇄*trans*-$[Ru(dmpe)_2(OCHO)_2]$).

Several possible CVs can be chosen to analyze the *cis*/*trans* isomerization of the catalyst complexes ($[Ru(dmpe)_2X_2]$, X = H or OCHO). One of the most efficient CVs for probing the change is the dihedral angle of the four phosphorus atoms, P(1)-P(2)-P(3)-P(4), in which P(1) and P(2) belong to one of the two dmpe ligands and P(3) and P(4) belong to the other. The dihedral angle alone, however, may be insufficient to clearly distinguish all possible *cis* and *trans* isomers because distinct positions of the two X ligands may correspond to the same dihedral. For example, the two X ligands can occupy the same coordination site to leave a vacancy on the opposite side. The different orientations of the X ligands can be taken into account by the bond angle X–Ru–X, which is therefore selected as a second CV.

The isomerization of $[Ru(dmpe)_2H_2]$ has been simulated starting from *cis*-$[Ru(dmpe)_2H_2]$ (**1**, Figure 2). The MTD trajectory explores for some time (3 ps) the basin of attraction of the initial configuration until the accumulation of the MTD potential induces a substantial change in the dihedral angle and the system transforms into the *trans* isomer **4**, crossing a barrier of about 20 kcal mol^{-1}. After a further two picoseconds of simulation time, the backward transition to the initial *cis* isomer **1** occurs along the same path and over a similar energy barrier. Once the two wells have been fully explored, an alternative route is found that connects two distinct, but equivalent, *cis* isomers **1**→**1′**. Indeed, the dihedral angle shown in Figure 2 is periodic and the *cis*-to-*cis* transition takes place through the negative direction of the dihedral angle axis. This pathway goes over a higher barrier of about 30 kcal mol^{-1}.

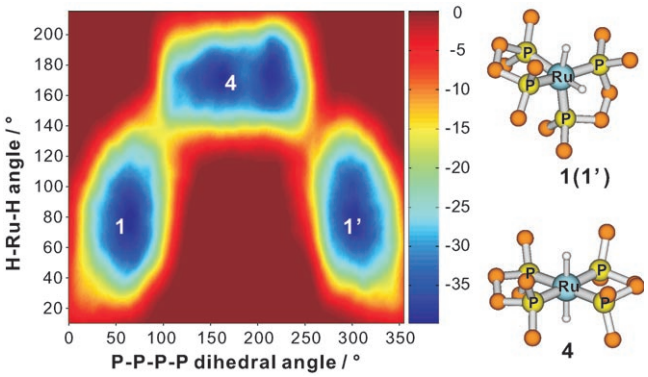

Figure 2. FES showing the *cis*/*trans* isomerization of $[Ru(dmpe)_2H_2]$ as a function of the dihedral angle of the four ligand phosphorus atoms and the H-Ru–H angle. The free energy is in kcal mol^{-1}. Representative structures near the minima, close to the numbered location on the FES, are shown on the right. For clarity the hydrogen atoms of the dmpe ligand are not shown.

With a sufficiently long MTD sampling the potential fills the three wells evenly until the trajectory can span the entire configurational space, moving over a barrierless energy landscape. The topology of the explored FES in the space of the CVs is then derived from the penalty potential accumulated during the exploration. The contour plot in Figure 2 clearly shows three stable configurations that correspond to the marked minima, which are the two distinguishable, but equivalent, *cis* complexes **1** and **1′** and *trans* complex **4**.

The relative probability of finding the system in the *trans* rather than in the *cis* isomeric form can be estimated from the ratio between the explored volumes of the configura-

tional space that correspond to the two structures. The *cis*/*trans* ratio obtained from the FES plotted in Figure 2 is roughly 2:1, which is an overestimate of the *trans* isomer, around 35%, compared with the experimental result, only 5.5% at 300 K in toluene.[52] This discrepancy can be accounted for by the fact that this study neglects the effect of solvent. The resulting increased mobility of the ligands might facilitate the isomerization, thus shifting the equilibrium towards the *trans* isomer.

The isomerization of the monoformate complex, [Ru(dmpe)$_2$H(OCHO)], was studied by using the dihedral angle and the bond angle of H–Ru–C (the carbon atom of the formate group) as CVs. The H–Ru–C angle is preferred to the H–Ru–O angle, in which oxygen is the atom that interacts with the ruthenium center directly, because of the formal equivalence of the two oxygen atoms of the formate group. Indeed, exchange of the coordinated oxygen atom by rotation of the formate group frequently occurs, as shown later, and causes large fluctuations in the H–Ru–O angle, although these changes do not correspond to real transitions of the structure of the complex.

We took the *cis* complex (**2**, Figure 3) as the initial configuration. After MTD (16 ps), we observed the first *cis*-to-*cis* rearrangement **2**→**2′** over a barrier of around 20 kcal mol^{-1}.

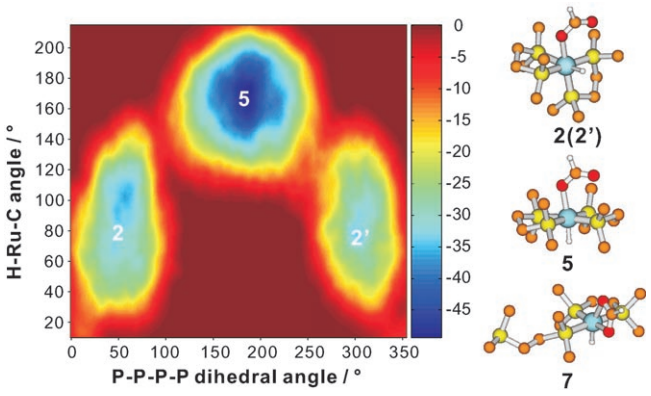

Figure 3. FES showing the *cis*/*trans* isomerization of [Ru(dmpe)$_2$H(OCHO)] as a function of the dihedral angle of the four ligand phosphorus atoms and the H-Ru–C (carbon atom of the formate group) angle. The free energy is in kcal mol^{-1}. Representative structures near the minima, close to the numbered location on the FES, are shown on the right. For clarity the hydrogen atoms of the dmpe ligand are not shown. Structure **7** was observed after filling the well of **5** and the FES was constructed by the hills deposited before the formation of **7**.

This rearrangement proceeded via an unstable complex characterized by the formate group, in which the hydride is located at the same coordination site. In this metastable configuration, the isomer temporarily becomes *trans* in which the dihedral angle is almost zero and the H–Ru–C angle is about ten degrees. The rearrangement is completed by going through an undercoordinated formate–metal state with a *trans*-like geometry, which is followed by a ligand rearrangement to a *cis* complex in which the ruthenium center is newly fully coordinated by the formate oxygen atom. Once the two energy wells of **2** and **2′** have been thoroughly explored, the higher transition state separating the *trans* from the *cis* isomers is reached and the transition occurs over a barrier of around 23 kcal mol^{-1} (**5**, Figure 3). Interestingly, the *trans* complex did not change back to *cis*, but rather one of the phosphorus atoms of the ligand dissociated and was replaced by the second oxygen atom of the formate, which completes the ruthenium coordination (**7**, Figure 3). The **5**→**7** energy barrier is estimated to be around 47 kcal mol^{-1}, which means that the *trans*→*cis* process, if possible, is expected to have an even higher activation energy.

The plot of the FES explored by MTD (Figure 3) clearly shows that the *trans* state is significantly more stable than the *cis*. This is in agreement with experimental results,[21] which indicates that *trans*-[Ru(dmpe)$_2$H(OCHO)] is very stable and almost the only complex observed at equilibrium. The fact that, starting from the monoformate complex, the *cis*→*cis* rearrangement is favored with respect to the expected *cis*→*trans* transition indicates that the isomerization process is less probable than in the case starting from the dihydride complex (Figure 2). This is likely because the formate group is bulkier than the hydride, which results in greater steric hindrance.

The formation of the two-oxygen coordinating complex, [Ru(dmpe)$_2$H(η^2-O$_2$CH)] was not detected experimentally and might well be an artifact of our model. The lack of interactions with the solvent may be one possible explanation for this behavior. Anyway, the energy barrier separating dissociated state **7** from *trans* complex **5** is very high, which implies that such a transition should not occur.

To investigate the isomerization of the diformate complex [Ru(dmpe)(OCHO)$_2$], we chose the C–Ru–C bond angle as the second CV in which the carbon atoms are those of the formate group. The *cis*-diformate complex turns out to be very stable. The MTD trajectory spends a long time fluctuating in the corresponding basin of attraction (ca. 11 ps) until one of the phosphorus atoms of the ligand dissociates. The energy barrier for the dissociation process was estimated to be around 50 kcal mol^{-1} and the product is the [Ru(dmpe)$_2$(OCHO)(η^2-O$_2$CH)] complex, which is similar to **7** in Figure 3. In this MTD simulation no *cis*→*trans* isomerization was observed. The pronounced steric effects induced by the two formate groups can be considered responsible for hindering the rotation of the ligands around the ruthenium atom, thereby preventing isomerization. The high stability of the *cis*-diformate complex, as predicted by our calculations, is in agreement with experimental observations, which shows that this complex is the most abundant formate complex under a CO$_2$ pressure in toluene at 300 K.[21]

CO$_2$ insertion/dissociation: A very facile CO$_2$ insertion into the dihydride complex was observed experimentally.[21,22] Two formate complexes, *cis*-diformate (**3**, Scheme 1) and *trans*-monoformate (**5**), were formed immediately after a CO$_2$ pressure of less than 5 bar at 300 K was applied.[21] In this subsection we address the reaction mechanisms and the

energetics of the insertion and dissociation processes starting from both the *cis* and the *trans* dihydride isomers. Based on mechanistic comparison between the *cis* and *trans* routes, we highlight some structural aspects that influence the overall reaction pathway.

To gain a complete description of the different steps along the CO_2 insertion/dissociation events we used three CVs. One efficient CV is the coordination number of oxygen atoms to the ruthenium center, CN(O) (Figure 1, dotted line). The second CV is the distance between the carbon atom of CO_2 and the hydrogen atom of the hydride, d(C–H). The third is the Ru-C-O angle in which the carbon and oxygen atoms belong to CO_2, $\measuredangle$(Ru–C–O). A repulsive potential wall is placed at 2.5 Å to limit d(C–H) and to prevent CO_2 from escaping from the simulation box. The artificial confinement can be regarded as a way to model the partial pressure of the gas phase. By its presence, we mimic the relatively high probability of a molecule in the vicinity of the ruthenium coordination shell. To consistently compare the free-energy profiles of different simulations, the location of the potential wall is the same for all of the systems.

Starting from *cis*-[Ru(dmpe)$_2$H$_2$], the MTD trajectory exhibits a rather quick transition process over a small barrier of around 6 kcal mol^{-1}. This first intermediate corresponds to the complex **1–2** (Figure 4), which is characterized by a significant interaction between CO_2 and the hydride.[21] The formate complex is formed in a concerted manner. Breaking the Ru–H bond and forming the Ru–O bond occur simultaneously by rotation of the formate group. Such a concerted mechanism was also predicted by static DFT calculations.[21] The low energy barrier of around 2 kcal mol^{-1} indicates that CO_2 insertion is almost immediate once the intermediate **1–2** has been stabilized. Three types of formate complexes have been observed that correspond to three different positions of the formate group relative to the ruthenium center. The transitions between them are driven by the third CV, that is, the angle $\measuredangle$(Ru–C–O′), in which O′ is the oxygen atom of CO_2 that has been selected to define the CV. In the first configuration, O′ does not coordinate to the ruthenium center and C–O′ points in the opposite direction, away from the ruthenium center ($\measuredangle$(Ru–C–O′)≈160°, **2** in Figure 4). In the second configuration, O′ does not coordinate directly to the ruthenium center, but interacts with the methyl group of the dmpe ligand ($\measuredangle$(Ru–C–O′)≈90°, **2′**). In the third configuration, O′ coordinates to the ruthenium center with an angle $\measuredangle$(Ru–C–O)≈30° (**2″**). Note that, in this last configuration, the formate can rotate around the Ru–O′–C axis, without changing the value of the CV. The MTD trajectory spends a long time exploring all of the broad region of the configurational space that corresponds to the formate complex. Finally, after 38 ps of simulation time, CO_2 dissociation occurs, crossing a much larger energy barrier of around 20 kcal mol^{-1}. The complete dissociation of CO_2 from the catalyst in the final step of the reverse pathway, that is, **1–2**→**1**, occurs with a barrier of around 4 kcal mol^{-1}.

Figure 4 shows the FES reconstructed from the MTD sampling of the initial CO_2 insertion and the reverse pathway (**1**⇔**2**). From the FES projected onto the plane of the CN and the d(C–H) variables (Figure 4a), we can identify the transition region at a C–H distance of about 1.4 Å.[53] The value of d(C–H) in **1–2** corresponds to the characteristic C–H bond length of the formate complexes (**2**, **2′**, and **2″**, Figure 4). Analysis of the bond character of **1–2**, based on the electron density distribution, shows that almost no Ru–H bond is present, whereas the C–H bond is practically already formed.[21] The three minima that correspond to the three observed formate complexes become distinguishable by projecting the three-dimensional FES onto the subspace defined by the Ru–C–O′ angle and the C–H distance (Figure 4b). From this perspective, we observe that there is almost no barrier between **2** and **2′**. In fact, the transition occurs by rotation of the formate group, but keeps the same coordinating oxygen. On the other hand, flipping the oxygen atoms (**2**, **2′** vs. **2″**, Figure 4) occurs with a barrier of around 10 kcal mol^{-1}.

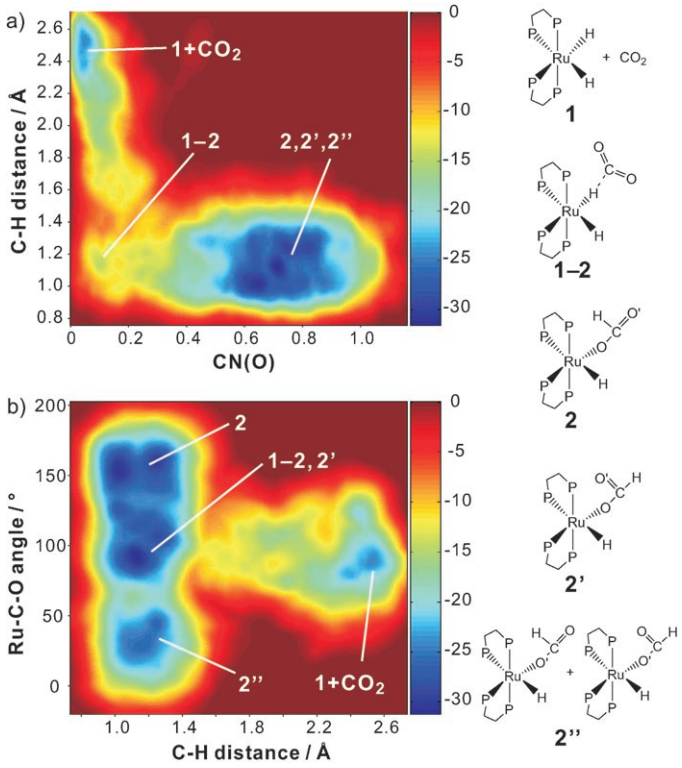

Figure 4. FES showing the processes of CO_2 insertion to *cis*-[Ru(dmpe)$_2$H$_2$] and CO_2 dissociation from *cis*-[Ru(dmpe)$_2$H(OCHO)] a) as a function of the coordination number (between the ruthenium and the oxygen atoms) and the C–H distance (the carbon atom of CO_2 or the formate group and the hydrogen atom of the hydride), and b) as a function of the C–H distance and the Ru–C–O angle (the carbon atom of CO_2 or the formate group and oxygen atom of one of the oxygen atoms of CO_2, marked as O′ on the right side). The free energy is in kcal mol^{-1}. Representative structures near the minima, close to the numbered location on the FES, are shown on the right.

According to structural and electronic properties, having one or other oxygen atom coordinating to the ruthenium center is equivalent; this implies that **2** plus **2′** and **2″** configurations should have the same statistical probability. Howev-

er, the MTD trajectory spends more time in one of the two wells, as inferred by the larger volume of the basin of **2** plus **2′** in Figure 4b. In fact, the two oxygen atoms (O and O′ in Figure 4) are not equivalent in our model because only O′ is directly involved in the definition of the CV; this might introduce a slight bias to the fluctuations of ∢(Ru–C–O). Most probably, a longer sampling time could adjust the balance between the two states. Nevertheless, complete sampling of the particular well (**2″**) will probably not change the overall characteristics of the free energy. The broad basin of attraction associated with the structures of **2**, **2′**, and **2″** makes this state very stable and kinetically favored. This explains why the reverse process towards **1–2** is a rather slow event with respect to the formation of the formate complex.

The second CO_2 insertion into *cis*-[Ru(dmpe)$_2$H(OCHO)] (**2**⇄**3**, Scheme 1) is characterized by a similar free-energy profile (Figure 5). CO_2 approaches the hydride with a small energy barrier (ca. 5 kcal mol^{-1}) and forms a complex similar to the intermediate that was observed during the first insertion (**2–3**, Figure 5a) in which CO_2 closely interacts with the hydride. The main difference between the first and second insertion is the position of the barrier, which is found at *d*(C–H) ≈ 1.6 Å rather than 1.4 Å. This change in position indicates that there is a larger effect of the steric hindrance of the formate complex compared with the dihydride catalyst. The transition to the final *cis*-diformate complex occurs by the same concerted insertion mechanism, over a small barrier of around 3 kcal mol^{-1}. Also for the diformate complex, we can distinguish three slightly different structures (**3**, **3′**, and **3″**) that correspond to different values of the ∢(Ru–C–O′) angle. The backward reaction mechanism from the diformate complex to the intermediate **2–3** proceeds over a barrier of around 16 kcal mol^{-1}, that is, less than in the case of the monoformate (ca. 20 kcal mol^{-1}). Complete CO_2 dissociation is slightly more demanding and requires around 7 kcal mol^{-1}.

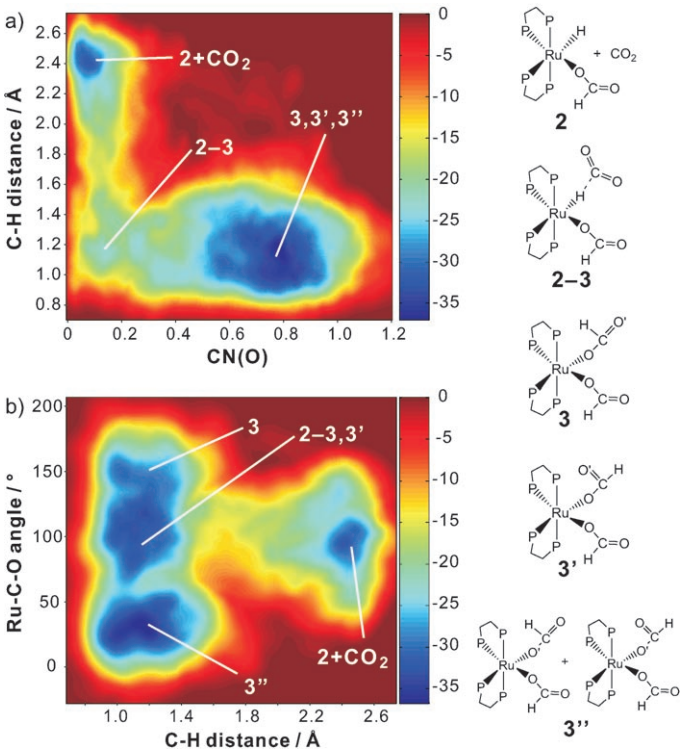

Figure 5. FES showing the processes of CO_2 insertion into *cis*-[Ru(dmpe)$_2$H(OCHO)] and CO_2 dissociation from *cis*-[Ru(dmpe)$_2$(OCHO)$_2$] a) as a function of the coordination number (between the ruthenium and the oxygen atoms) and the C–H distance (the carbon atom of CO_2 or the formate group and the hydrogen atom of the hydride), and b) as a function of the C–H distance and the Ru–C–O angle (the carbon atom of CO_2 or the formate group and the oxygen atom of one of the oxygen atoms of CO_2, marked as O′ in the structures shown on the right). The free energy is in kcal mol^{-1}. Representative structures near the minima, close to the numbered location on the FES, are shown on the right.

The similarity between the two processes is seen clearly by analysis of the FES. The projection of the surface onto the plane of *d*(C–H) and ∢(Ru–C–O) (Figure 5b) shows that the internal rotation of the formate group, from **3** to **3′**, is almost barrierless. Alternatively, flipping of the oxygen atom, which leads to configuration **3″**, requires an activation energy of around 10 kcal mol^{-1}. The two separated wells, that is, **3** plus **3′** and **3″,** respectively, are roughly equivalent in size, which indicates that there is an evenly distributed probability of either one of the two formate oxygen atoms interacting with the ruthenium center.

To study CO_2 insertion/dissociation into the *trans*-dihydride isomer, **4**⇄**5** in Scheme 1, we used the same MTD setup. We obtained a rather different mechanism compared with the *cis* route, with an additional intermediate state for the approaching CO_2 molecule at a distance *d*(C–H) of about 1.7 Å. From this minimum, first a closely interacting complex with CO_2 (**4–5**, Figure 6) is formed crossing a barrier of 5 kcal mol^{-1} and finally CO_2 insertion is completed over a barrier of around 4 kcal mol^{-1}. Once one of the three *trans*-formate complexes (**5**, **5′**, and **5″**) is formed, we observe rather large fluctuations in CN(O). These fluctuations indicate an enhanced mobility of the formate group that interacts with the ruthenium center compared with the same molecule interacting with the *cis* isomer. The backward transition to the intermediate **4–5** occurs by rotation of the formate group with a barrier of around 5 kcal mol^{-1}, which is much lower than for the *cis* cases discussed above. The final dissociation from **4–5** to **4** (Figure 6) requires around 6 kcal mol^{-1}.

The explored FES (Figure 6) exhibits considerably shallower wells, which indicates that all of the elementary processes occur rapidly over the smoother energy landscape. The additional intermediate becomes visible by projecting the FES onto the *d*(C–H) and CN(O) plane (Figure 6a). The larger coordination space and the reduced steric hindrance that characterizes the *trans* complex explain why this intermediate is not found during CO_2 insertion into the *cis* isomer. The resulting stepwise mechanism enhances the concentration of CO_2 near the hydride, which facilitates CO_2 insertion. Extension of the well to low CN(O) values reflects the greater mobility of the formate group and implies that the *trans*-formate complex is stable even at rather large dis-

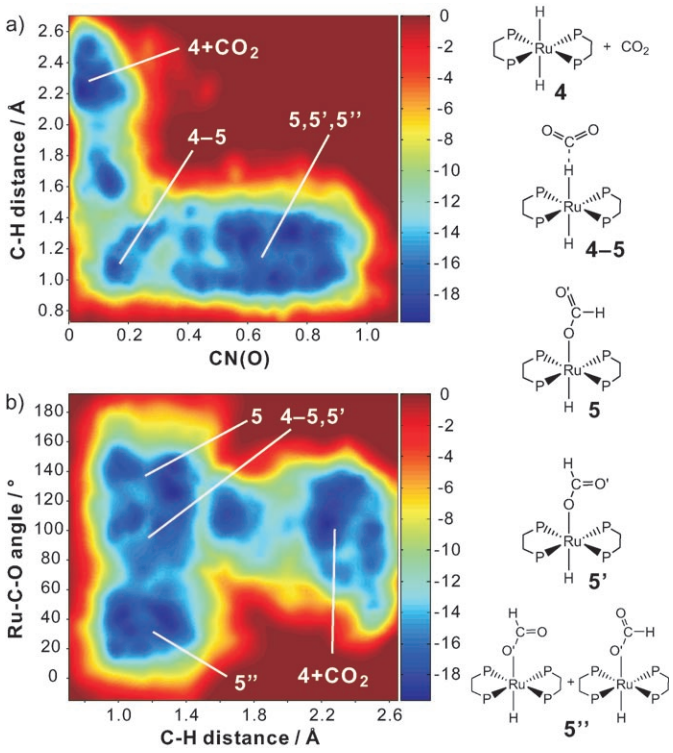

Figure 6. FES showing the processes of CO_2 insertion into *trans*-[Ru(dmpe)$_2$H$_2$] and CO_2 dissociation from *trans*-[Ru(dmpe)$_2$H(OCHO)] a) as a function of the coordination number (between the ruthenium and the oxygen atoms) and the C–H distance (the carbon atom of CO_2 or the formate group and the hydrogen atom of the hydride), and b) as a function of the C–H distance and the Ru–C–O angle (the carbon atom of CO_2 or the formate group and the oxygen atom of one of the oxygen atoms of CO_2, marked as O′ in the structures shown on the right). The free energy is in kcal mol^{-1}. Representative structures near the minima, close to the numbered location on the FES, are shown on the right.

tances of the formate group from the ruthenium center. The value of 0.4 for the CN(O) corresponds to a Ru–O length of 2.7 Å (Figure 1), which is significantly longer than the equilibrium distance of the formate complex (2.3 Å). Moreover, we observe that the internal rotation of the formate group, that is, **5**→**5′** (Figure 6), is almost barrierless, whereas a smaller barrier of 4 kcal mol^{-1} is found for flipping of the oxygen (**5**, **5′** vs. **5″**, Figure 6). The long-range stability of the formate group seems to affect and facilitate the CO_2 dissociation process.

In summary, the MTD analysis has revealed a rather high reaction rate for the insertion of CO_2 by either route, *cis* or *trans*, which is in excellent agreement with experimental observations.[21,22] The dissociation process is more difficult for *cis* complexes, whereas it is as facile as the insertion process for the *trans* complex. The overall lower barriers for the *trans* complex relative to the *cis* complexes confirm the results obtained by static DFT investigations.[21] In all three cases, once the C–H bond is formed, CO_2 insertion/dissociation occurs by rotation of the formate group at a constant C–H distance. Natural bond orbital analysis[54] of the intermediate complexes suggests that the formate group can behave like an ionic species. Indeed, it exhibits a highly ionic character and its electronic structure is nearly identical to that of the formate ion.[21] This picture accounts for the weak interactions between the "rotating formate ion" and the ruthenium center, which in turn favor the structural rearrangements of the formate complexes.[21]

Formation of formic acid and its reaction with the dihydride catalyst: From experimental evidence, we know that under high H_2 pressure, the formate complexes transform into *trans*-dihydride complexes that interact with formic acid (Scheme 1).[21] As soon as the H_2 pressure is lowered, the formic acid reacts with the dihydride catalyst and the original *trans*-monoformate complex is recovered,[21] which implies that H_2 insertion and the formic acid reaction are reversible and in equilibrium (**5**⇔**6**, Scheme 1).[55] Only the *trans*-dihydrogen-bonded complex has been detected experimentally, whereas no *cis* equivalent has been found.

In this section we report the results of our MTD study of the fundamental steps of the H_2 insertion/formic acid reaction processes, which were unknown until now. We consider both the *cis* and the *trans* cases and carefully analyze the different intermediates to understand why only the *trans* route seems to be possible according to experimental analysis. The simulations were carried out by using two CVs. They are the coordination numbers for oxygen CN(O) (Figure 1, solid line) and hydrogen CN(H) (Figure 1, –•–•) at the ruthenium center. Confinement potentials were employed to guarantee that the H_2 molecule, the formate group, and the formic acid remain within a limited distance of the ruthenium center.

Starting from the separated *cis*-formate complex and the hydrogen molecule (**2**, Figure 7), the lowest energy path for H_2 insertion is via **8** in which both H_2 and the formate group distantly interact with the ruthenium center.[56] The next step is the formation of a [Ru(η^2-H$_2$)] complex (**9**, Figure 7) in which the molecular hydrogen coordinates to the ruthenium center giving a global CN(H) approximately equal to 3. This class of η^2-H_2 complex has been increasingly reported[57,58] and it turns out that these complexes are important as intermediates in various hydrogenation reactions.[59–62] This complex has been identified as an energetic minimum and not a transition state.[21] In the final step, the formic acid is formed and stabilized by the dihydrogen-bonding interaction (**10**, Figure 7). Examples of dihydrogen-bonding complexes formed via an η^2-H_2 intermediate have already been reported in the literature.[63–67]

Figure 7 shows the FES for H_2 insertion into the *cis*-monoformate complex (**2**→**10**) and of the backward reaction, that is, the reaction of formic acid with the *cis*-dihydride catalyst, which results in the formation of the formate complex and H_2 (**10**→**2**).[68] Unfortunately, in this representation, the pathway **8**→**9** is hardly visible because it overlaps with the basin of attraction of **10**. More information about the energetics of the observed mechanism between **8** and **9** can be inferred directly from the Kohn–Sham energy profile along the trajectory. The fast fluctuations of the systems from one

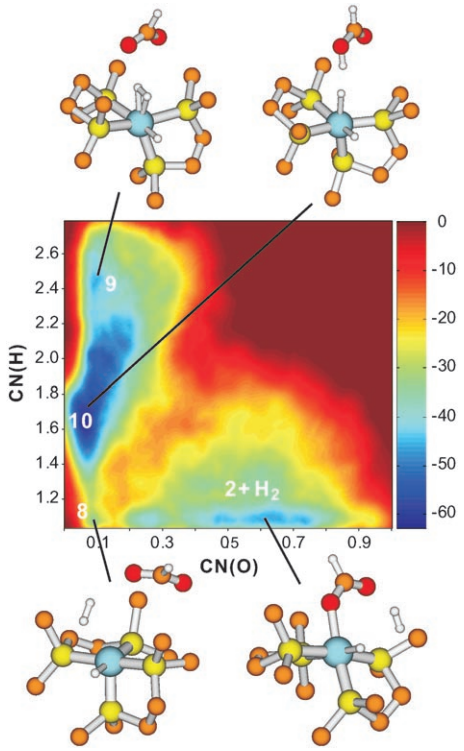

Figure 7. FES showing the processes of H_2 insertion into *cis*-[Ru(dmpe)$_2$H(OCHO)] and the formic acid reaction with *cis*-[Ru(dmpe)$_2$H$_2$] as a function of the coordination number between the ruthenium and the oxygen atoms and between the ruthenium and the hydrogen atoms. The free energy is in kcal mol^{-1}. Representative snapshots of structures near the minima, close to the numbered location on the FES, are also shown. For clarity the hydrogen atoms of the dmpe ligand are not shown.

state to the other are associated with small variations in the potential energy, which suggests a rather shallow free-energy landscape. Hence the free-energy contribution of this fast fluctuating mode is neglected in the further interpretation of the FES. H_2 insertion (**2**→**9** via **8**) proceeds over a barrier of 22 kcal mol^{-1}. By choosing different positions for the confinement potential, we can affect the behavior of the reacting system. By setting the minimum value to 1.05 for CN(H), we force the H_2 molecule to remain very close to the ruthenium center, thus reproducing the experimental conditions of a high concentration of H_2. As a side effect, this might slightly destabilize the whole complex to result in a shallower free-energy well for **2**. This effect can be used to understand the properties of the formate complex under high H_2 pressure better. The final reaction step from **9**→**10** passes through a very low barrier of around 3 kcal mol^{-1}.

The backward reaction (**10**→**2**, Figure 7) follows exactly the same two-step pathway, **10**→**9** (18 kcal mol^{-1}) and **9**→**2** via **8** (22 kcal mol^{-1}). A similar destabilization effect to that described for the forward reaction is likely to be induced by the confinement potential applied to the CN(O) CV. As a result, the **10**→**9** transition barrier is probably underestimated (Figure 7).

The mechanism disclosed by the MTD starting from the *trans* complex proceeds through four similar structures (**5**, **11**, **12**, and **6**, Figure 8). The same wall potential was used for the CN(O), whereas a different minimum value was chosen for CN(H) (at 0.18) owing to the different number

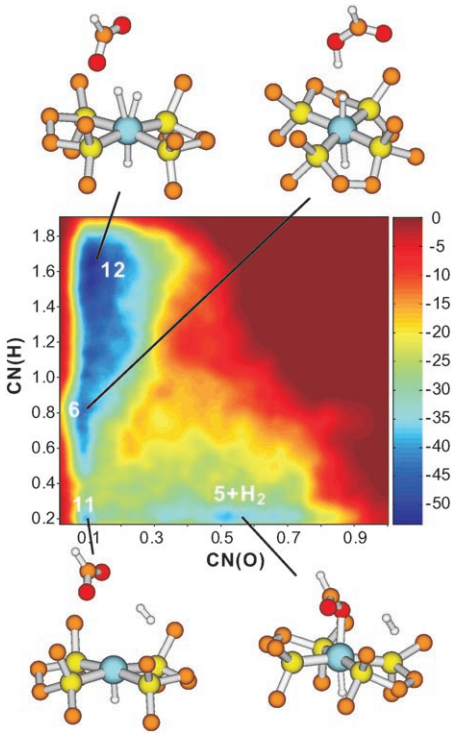

Figure 8. FES showing the processes of H_2 insertion into *trans*-[Ru(dmpe)$_2$H(OCHO)] and the formic acid reaction with *trans*-[Ru(dmpe)$_2$H$_2$] as a function of the coordination number between the ruthenium and the oxygen atoms and between the ruthenium and the hydrogen atoms. The free energy is in kcal mol^{-1}. Representative snapshots of structures near the minima, close to the numbered location on the FES, are also shown. For clarity the hydrogen atoms of the dmpe ligand are not shown.

of hydrogen atoms involved in the reaction path (two for the *trans*, Figure 8, and three for the *cis*, Figure 7). Several remarkable differences between the *cis* and *trans* routes were observed. The stationary points on the FES are somewhat displaced and show different relative stabilities. In particular, the *trans* isomer of the [Ru(η^2-H$_2$)] complex is significantly more stable (Figure 7 and Figure 8).

The free-energy well of the *trans*-formate complex is centered at a much lower CN(O) value. Consequently, the cross-section between the well of **5** and the well formed by **12** and **6** is larger for the *trans* route than the *cis* route, that is, between the well of **2** and the well of **9** and **10** (Figure 7), and hence, a larger channel between the minima is to be expected for the *trans* route. The wide and shallow transition channel suggests that the H_2 insertion step occurs with a higher probability by the *trans* route (**5**→**12**, Figure 8) than by the *cis* route (**2**→**9**, Figure 7). The fluctuations of CN(O) towards the lower value in the *trans* route can also be seen from the CO_2 insertion/dissociation steps shown in Figure 4

and Figure 6. This fluctuation indicates that the formate group has a wider stability range in the *trans* form, which increases the statistical weight of the *trans* isomer making the backward reaction, that is, CO_2 dissociation, more difficult.

In contrast to what is observed along the *cis* route, the equilibrium between **12** and **6** is shifted towards **12** for the *trans* complex (Figure 8). The static DFT calculations showed that the interaction of the formic acid with the dihydride through dihydrogen bonding is stronger when the complex is in the *trans* form (8.0 kcal mol^{-1}) rather than in the *cis* form (6.3 kcal mol^{-1}).[21] This means that the formic acid should interact, and hence, react more easily along the *trans* route. Moreover, the difference in potential energy between the *trans*-[Ru(η^2-H_2)] complex and the more stable dihydrogen-bonding complex is only 3.4 kcal mol^{-1} compared with 7.2 kcal mol^{-1} calculated for the *cis* equivalent. This energy difference implies that the formic acid is stabilized along the *cis* route more.[21] These two factors may be at the origin of the difference in the equilibrium between the [Ru(η^2-H_2)] complex (**9** or **12**) and the dihydrogen-bonded complex (**10** or **6**).

Furthermore, H_2 insertion into the formate complex (**5**→**12**, Figure 8) occurs with a barrier of around 10 kcal mol^{-1}, which is significantly lower than the barrier in the *cis* route (22 kcal mol^{-1}). Surprisingly, no energy barrier could be detected for hydrogen transfer from [Ru(η^2-H_2)] to the formate along the **12**→**6** step (Figure 8) and dihydrogen-bonded complex **6** turned out to be 5 kcal mol^{-1} less stable than the [Ru(η^2-H_2)] complex **12**.[69] Moreover, the backward reaction by the *trans* route occurs more easily than along the *cis* route. The first backward reaction step, the formation of the [Ru(η^2-H_2)] complex (**6**→**12**, Figure 8), is practically barrierless, whereas the following step, H_2 dissociation and formate coordination, proceeds over a barrier of 22 kcal mol^{-1} (**12**→**5**, Figure 8), which is similar to that observed for the *cis* route.

A reasonable estimate of the relative probability of the two competitive routes can be proposed on the basis of the FES profile. In particular, the fact that wider transition channels are available for the *trans* route, together with a greater flexibility during the atomic rearrangements, makes this reaction process more probable.

Overall reaction pathways: The overall picture of the pathways and the free-energy barriers of each reaction step obtained from the MTD investigations are summarized in Scheme 2.[70] It turns out that the target reaction, that is,

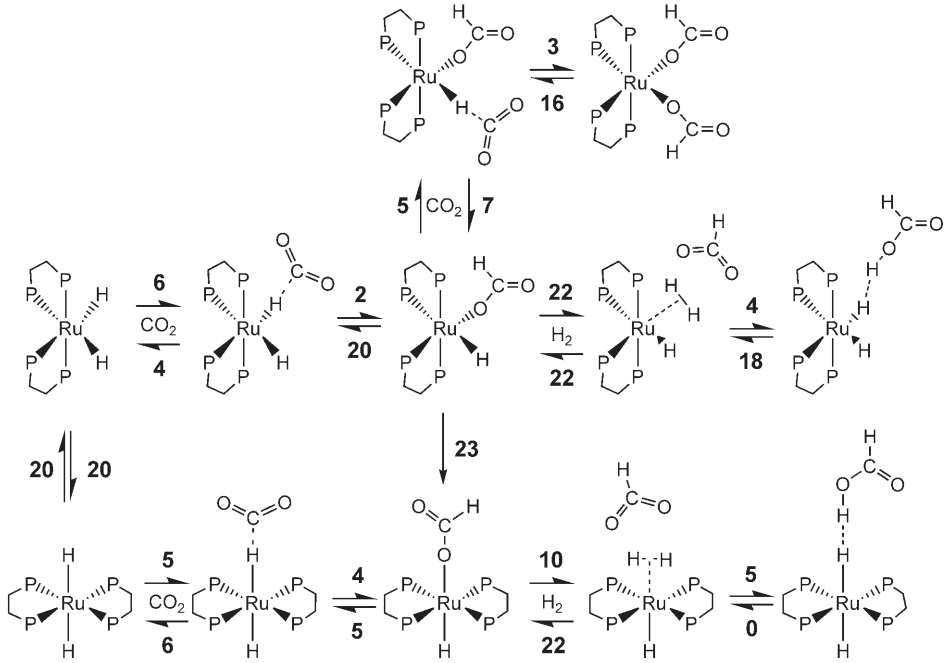

Scheme 2. Overall reaction pathways and free-energy barriers obtained by the metadynamics simulation. The free-energy barriers are given in kcal mol^{-1}.

CO_2 insertion followed by formic acid formation, should preferentially occur by the *trans* route. The rate-limiting step of the reaction is H_2 insertion into the formate complex and the formation of the *trans*-[Ru(η^2-H_2)] complex. The latter is expected to have a rather short lifetime because the energy barrier for the following hydrogen transfer to the formate oxygen is only 5 kcal mol^{-1}. This would explain why the [Ru(η^2-H_2)] complex has not been observed in our experimental study, whereas the dihydrogen-bonded complex was observed under high H_2 pressure.[21]

The first and second CO_2 insertions by the *cis* route are as facile as by the *trans* route. This result is in agreement with the IR experimental spectra in which both the *cis*-[Ru(dmpe)$_2$(OCHO)$_2$] and *trans*-[Ru(dmpe)$_2$H(OCHO)] complexes are observed at 300 K.[21,22] A significantly higher barrier to H_2 insertion (22 kcal mol^{-1}) is found instead along the *cis* route. The insertion should therefore proceed by the *trans* route, which is also kinetically favored as a result of the wider channel that characterizes the underlying FES.

Experiments show that under moderate CO_2 pressure (5 bar) at 300 K in toluene, the *cis*-[Ru(dmpe)$_2$(OCHO)$_2$] complex predominates.[21] When high H_2 pressure (>50 bar) is applied in addition to the moderate CO_2 pressure (5 bar), the equilibrium balance is reversed in favor of the *trans* isomer and mainly the dihydrogen-bonded complex *trans*-[Ru(dmpe)$_2$H$_2$]···HOCHO is detected.[21] The free-energy

barriers reported in Scheme 2 are consistent with experimental observations. The equilibrium between the *trans*-monoformate complex (**5**, Scheme 1) and *trans*-dihydrogen-bonded complex **6** is shifted towards the latter under high H_2 pressure. The lowest-energy pathway to the *trans*-monoformate complex from *cis*-diformate complex **3** involves the dissociation of CO_2 followed by the *cis*→*trans* isomerization of the dihydride catalyst and CO_2 insertion. This process would lead, in time, to the predominant presence of the *trans* isomer.

By introducing formic acid into the dihydride complex solution at 300 K, the only species to be detected is the *trans*-monoformate complex (**4**→**5**, Scheme 1).[21] This observation can be explained by our results which demonstrate that the coordination of the hydrogen atom of formic acid to the ruthenium center takes place spontaneously by the *trans* route (Scheme 2, right to left), whereas it proceeds over a relatively high barrier by the *cis* route. Moreover, the *trans* route is kinetically favored, as shown by a broader and smoother transition region on the FES, which can be explained by the wider approach channel offered by the open structure of the *trans* isomer. The *cis* route also seems possible from Scheme 2 and the *cis*-monoformate complex is likely produced, but it was not observed at 300 K, most likely owing to its low stability.[22] The *cis*-monoformate complex may transform into the *trans* complex by two alternative pathways: 1) Direct isomerization or 2) CO_2 dissociation followed by *cis*→*trans* isomerization and the reaction with formic acid. The latter pathway is slightly favored according to our estimate of the activation barriers.

Ligand effects and towards rational catalyst design: Comparison of the competitive reaction mechanisms, taking into consideration energetic profiles as well as some kinetic aspects, seems to indicate that the *trans* routes are the preferred ones. The rate-limiting step turns out to be H_2 insertion, no matter which route is taken. The corresponding transition state within the *trans* route, **11** in Figure 8, is characterized by the approaching molecular hydrogen, which induces weakening of the Ru–formate interaction, and by the consequent displacement of the formate group to larger distances. Analysis of the electronic structure confirms that the high-energy barrier originates from the destabilization of the formate group caused by the loose interaction between the oxygen atom and the Ru–H bond.[21] The "formate ion"-like species is clearly revealed in the proximity of the transition state of H_2 insertion as well as that of CO_2 insertion.

The correlation between the different ligands and the activity of the catalyst can be derived from the specific electronic structure of the transition state. One of the simplest measures is the stability of the formate ion near the Ru^+ center, in other words, the binding energy of the formate complex in which the Ru^+ complex and the formate ion are considered as the building blocks. When binding between the ions is weaker, the barrier height at the transition state is expected to be lower, that is, the smaller the binding energy is, the higher the activity. The binding energies between the *trans* catalyst with four different ligands (dmpe, PMe_3, dppe (dppe = PPh_2–CH_2CH_2–PPh_2), and X (X = HMeP–CH_2CH_2–PHMe)) and the formate are compared in Table 1. Ligand X is similar to dmpe and has a structure in which one of the dmpe methyl groups is substituted by a hydrogen atom. The binding energy increases in the order dppe < PMe_3 < dmpe < X. It is difficult to compare this trend directly with the activities reported in literature because they were measured under different experimental conditions (concentration, temperature, and additives). However, the general trend indicates that the activity of the catalyst towards formic acid formation progressively decreases in the sequence dppe > PMe_3 > dmpe > X.[12,13,15] In fact, the activity data for the catalyst with ligand X has not been measured, but it is expected to be almost zero, as is the case when one methyl group of dppe is substituted by a hydrogen atom.[15] The binding energy versus activity relationship confirms that, in spite of its bulkier structure, the dppe complex is one of the most efficient catalysts because of the weak binding of the formate group. Note that the superior activity of the dppe complex suggested by our calculations fully agrees with earlier experimental observations in which the dppe complex was found to be the most active of various Ru–bidentate complexes (e.g., dppm and dppp) for *N*,*N*-dimethylformamide synthesis from CO_2.[13] The related softening of the mode favors the stabilization of the formate at larger distances from the ruthenium center and consequently its ionic character. Therefore, it can be concluded that the electronic structure of the catalyst affects its activity more than steric hindrance.

Table 1. Binding energies of the formate group of various ruthenium catalysts with different ligands.[a]

Ru^+ complex	Binding energy [kcal mol^{-1}]
trans-[Ru(dmpe)$_2$H]$^+$	112.4
trans-[Ru(PMe$_3$)$_4$H]$^+$	111.6
trans-[Ru(dppe)$_2$H]$^+$	99.7
trans-[RuX$_2$H]$^+$	116.1

[a] The abbreviations for the ligands are: dppe = PPh_2–CH_2CH_2–PPh_2 and X = HMeP–CH_2CH_2–PHMe. The zero-point energies are corrected.

Conclusion

Practically relevant reaction pathways for the homogeneous catalytic CO_2 hydrogenation have been investigated by ab initio MTD by using [Ru(dmpe)$_2$H$_2$] as a model catalyst. Several aspects that cannot be addressed by static electronic structure calculations were studied by molecular dynamics. Our work reproduced the actual dynamic mechanisms that lead to isomerization and CO_2 insertion/dissociation at a finite temperature. We explored the role of entropic effects, which contribute to the most probable pathway and the relative stability of the intermediate states. Previously unforeseen structures have been observed and their influence on

the reaction rates has been discussed. The simulations presented in this work answer several open questions relating to the reaction system under study. It has been established that CO_2 insertion occurs by a concerted mechanism that involves the rotation of the formate group. Several interesting intermediates have been encountered along the reactive trajectories, for example, the complex with molecular H_2 coordinated to $[Ru(\eta^2\text{-}H_2)]$. The most relevant structures have been described in detail and their relative stability has been discussed in terms of the interatomic interactions and the associated electronic charge distribution. The free-energy profiles reconstructed by the MTD are consistent with experimental results and provide a more precise interpretation of the observed behavior. Finally, we conclude that the reaction proceeds more easily by the *trans* isomer route and that H_2 insertion into the formate complex is the rate-limiting step of the reaction. On the basis of the disclosed reaction pathways, a procedure that predicts the activity of catalysts with different ligands has been proposed. By this simple measure, derived from the analysis of the FES in the proximity of the rate-limiting step, the activity of the catalyst with different ligands can be easily estimated. The combination of in situ spectroscopic work, carried out under reaction conditions, and ab initio MTD has proven to be an extremely powerful tool for the characterization of unknown pathways and the interpretation of reaction processes that are not fully understood. The resulting atomistic picture can provide helpful hints for engineering improved reaction systems. In particular, the reaction pathways elucidated in this work can be of great help in understanding other effects, such as the influence of additives.

Acknowledgements

Computational time at ETH Zurich and CSCS, Manno, Switzerland, and financial support from the Foundation Claude and Giuliana are kindly acknowledged.

[1] C. Song, *Catal. Today* **2006**, *115*, 2–32.
[2] I. Omae, *Catal. Today* **2006**, *115*, 33–52.
[3] Kyoto Protocol to the United Nations Framework Convention on Climate Change, Kyoto, **1997**.
[4] *Climate Change 2001: The Scientific Basis*, (Eds.: J. T. Houghton, Y. Ding, D. J. Griggs, M. Noguer, P. J. van der Linden, X. Dai, K. Maskell, C. A. Johnson), Cambridge University Press, Cambridge, **2001**.
[5] W. Leitner, *Coord. Chem. Rev.* **1996**, *153*, 257–284.
[6] A. Baiker, *Appl. Organomet. Chem.* **2000**, *14*, 751–762.
[7] H. Arakawa, M. Aresta, J. N. Armor, M. A. Barteau, E. J. Beckman, A. T. Bell, J. E. Bercaw, C. Creutz, E. Dinjus, D. A. Dixon, K. Domen, D. L. DuBois, J. Eckert, E. Fujita, D. H. Gibson, W. A. Goddard, D. W. Goodman, J. Keller, G. J. Kubas, H. H. Kung, J. E. Lyons, L. E. Manzer, T. J. Marks, K. Morokuma, K. M. Nicholas, R. Periana, L. Que, J. Rostrup-Nielson, W. M. H. Sachtler, L. D. Schmidt, A. Sen, G. A. Somorjai, P. C. Stair, B. R. Stults, W. Tumas, *Chem. Rev.* **2001**, *101*, 953–996.
[8] M. Aresta, A. Dibenedetto, *Catal. Today* **2004**, *98*, 455–462.
[9] P. G. Jessop, Y. Hsiao, T. Ikariya, R. Noyori, *J. Am. Chem. Soc.* **1994**, *116*, 8851–8852.
[10] P. G. Jessop, T. Ikariya, R. Noyori, *Nature* **1994**, *368*, 231–233.
[11] P. G. Jessop, T. Ikariya, R. Noyori, *Science* **1995**, *269*, 1065–1069.
[12] P. G. Jessop, Y. Hsiao, T. Ikariya, R. Noyori, *J. Am. Chem. Soc.* **1996**, *118*, 344–355.
[13] O. Kröcher, R. A. Köppel, A. Baiker, *Chem. Commun.* **1997**, 453–454.
[14] O. Kröcher, R. A. Köppel, A. Baiker, *Chimia* **1997**, *51*, 48–51.
[15] C. C. Tai, J. Pitts, J. C. Linehan, A. D. Main, P. Munshi, P. G. Jessop, *Inorg. Chem.* **2002**, *41*, 1606–1614.
[16] C. A. Thomas, R. J. Bonilla, H. Yong, P. G. Jessop, *Can. J. Chem.* **2001**, *79*, 719–724.
[17] P. Munshi, A. D. Main, J. C. Linehan, C. C. Tai, P. G. Jessop, *J. Am. Chem. Soc.* **2002**, *124*, 7963–7971.
[18] J. C. Tsai, K. M. Nicholas, *J. Am. Chem. Soc.* **1992**, *114*, 5117–5124.
[19] Y. Musashi, S. Sakaki, *J. Am. Chem. Soc.* **2000**, *122*, 3867–3877.
[20] Y. Y. Ohnishi, T. Matsunaga, Y. Nakao, H. Sato, S. Sakaki, *J. Am. Chem. Soc.* **2005**, *127*, 4021–4032.
[21] A. Urakawa, F. Jutz, G. Laurenczy, A. Baiker, *Chem. Eur. J.* **2007**, *13*, 3886–3899.
[22] M. K. Whittlesey, R. N. Perutz, M. H. Moore, *Organometallics* **1996**, *15*, 5166–5169.
[23] A. Laio, M. Parrinello, *Proc. Natl. Acad. Sci. U.S.A.* **2002**, *99*, 12562–12566.
[24] M. Iannuzzi, A. Laio, M. Parrinello, *Phys. Rev. Lett.* **2003**, *90*, 238302.
[25] R. Martonak, A. Laio, M. Parrinello, *Phys. Rev. Lett.* **2003**, *90*, 075503.
[26] A. Stirling, M. Iannuzzi, A. Laio, M. Parrinello, *ChemPhysChem* **2004**, *5*, 1558–1568.
[27] A. Stirling, M. Iannuzzi, M. Parrinello, F. Molnar, V. Bernhart, G. A. Luinstra, *Organometallics* **2005**, *24*, 2533–2537.
[28] A. R. Oganov, R. Martonak, A. Laio, P. Raiteri, M. Parrinello, *Nature* **2005**, *438*, 1142–1144.
[29] T. Ikeda, M. Hirata, T. Kimura, *J. Chem. Phys.* **2005**, *122*, 244507.
[30] M. Pagliai, M. Iannuzzi, G. Cardini, M. Parrinello, V. Schettino, *ChemPhysChem* **2006**, *7*, 141–147.
[31] A. Rodriguez-Fortea, M. Iannuzzi, M. Parrinello, *J. Phys. Chem. B* **2006**, *110*, 3477–3484.
[32] A. Laio, A. Rodriguez-Fortea, F. L. Gervasio, M. Ceccarelli, M. Parrinello, *J. Phys. Chem. B* **2005**, *109*, 6714–6721.
[33] C. Micheletti, A. Laio, M. Parrinello, *Phys. Rev. Lett.* **2004**, *92*, 170601.
[34] B. Ensing, A. Laio, M. Parrinello, M. L. Klein, *J. Phys. Chem. B* **2005**, *109*, 6676–6687.
[35] G. Bussi, A. Laio, M. Parrinello, *Phys. Rev. Lett.* **2006**, *96*, 090601.
[36] B. Ensing, M. De Vivo, Z. W. Liu, P. Moore, M. L. Klein, *Acc. Chem. Res.* **2006**, *39*, 73–81.
[37] R. Car, M. Parrinello, *Phys. Rev. Lett.* **1985**, *55*, 2471–2474.
[38] F. L. Gervasio, A. Laio, M. Iannuzzi, M. Parrinello, *Chem. Eur. J.* **2004**, *10*, 4846–4852.
[39] F. L. Gervasio, A. Laio, M. Parrinello, M. Boero, *Phys. Rev. Lett.* **2005**, *94*, 158103.
[40] F. L. Gervasio, A. Laio, M. Parrinello, *J. Am. Chem. Soc.* **2005**, *127*, 2600–2607.
[41] A. Barducci, R. Chelli, P. Procacci, V. Schettino, F. L. Gervasio, M. Parrinello, *J. Am. Chem. Soc.* **2006**, *128*, 2705–2710.
[42] C. Ceriani, A. Laio, E. Fois, A. Gamba, R. Martonak, M. Parrinello, *Phys. Rev. B* **2004**, *70*, 113403.
[43] CPMD, Copyright IBM Corp., **1990–2006**; Copyright MPI für Festkörperforschung, Stuttgart, **1997—2001**; http://www.cpmd.org.
[44] A. D. Becke, *Phys. Rev. A* **1988**, *38*, 3098–3100.
[45] J. P. Perdew, *Phys. Rev. B* **1986**, *33*, 8822–8824.
[46] N. Troullier, J. L. Martins, *Phys. Rev. B* **1991**, *43*, 1993–2006.
[47] R. W. Hockney, *The Potential Calculation and Some Applications*, Academic Press, New York, London, **1970**, vol. 9.
[48] A. D. Becke, *J. Chem. Phys.* **1993**, *98*, 5648–5652.
[49] J. P. Perdew, Y. Wang, *Phys. Rev. B* **1992**, *45*, 13244–13249.
[50] Gaussian 03, Revision C.02, M. J. Frisch, G. W. Trucks, H. B. Schlegel, G. E. Scuseria, M. A. Robb, J. R. Cheeseman, J. A. Montgomery, Jr., T. Vreven, K. N. Kudin, J. C. Burant, J. M. Millam, S. S. Iyen-

gar, J. Tomasi, V. Barone, B. Mennucci, M. Cossi, G. Scalmani, N. Rega, G. A. Petersson, H. Nakatsuji, M. Hada, M. Ehara, K. Toyota, R. Fukuda, J. Hasegawa, M. Ishida, T. Nakajima, Y. Honda, O. Kitao, H. Nakai, M. Klene, X. Li, J. E. Knox, H. P. Hratchian, J. B. Cross, C. Adamo, J. Jaramillo, R. Gomperts, R. E. Stratmann, O. Yazyev, A. J. Austin, R. Cammi, C. Pomelli, J. Ochterski, P. Y. Ayala, K. Morokuma, G. A. Voth, P. Salvador, J. J. Dannenberg, V. G. Zakrzewski, S. Dapprich, A. D. Daniels, M. C. Strain, O. Farkas, D. K. Malick, A. D. Rabuck, K. Raghavachari, J. B. Foresman, J. V. Ortiz, Q. Cui, A. G. Baboul, S. Clifford, J. Cioslowski, B. B. Stefanov, G. Liu, A. Liashenko, P. Piskorz, I. Komaromi, R. L. Martin, D. J. Fox, T. Keith, M. A. Al-Laham, C. Y. Peng, A. Nanayakkara, M. Challacombe, P. M. W. Gill, B. Johnson, B. Chen, M. W. Wong, C. Gonzalez, J. A. Pople, Gaussian, Inc., Pittsburgh, PA, **2004**.

[51] L. D. Field, T. W. Hambley, B. C. K. Yau, *Inorg. Chem.* **1994**, *33*, 2009–2017.

[52] Field and co-workers reported a higher *trans* isomer concentration (ca. 7.7%) in toluene at 240 K, see ref. [51].

[53] Note that the minimum appearing at $d(C-H) = 2.5$ Å does not really correspond to a highly probable configuration, but is an effect of the confinement potential set at this distance.

[54] F. Weinhold, C. Landis, *Valency and Bonding*, Cambridge University Press, Cambridge, **2005**.

[55] The backward reaction (**6**→**5**) takes place in the absence of base, which would otherwise extract the dihydrogen-bonded formic acid from the catalyst and promote the reaction by shifting the equilibrium towards **5**→**6**.

[56] This process is similar to the reported ligand displacement by molecular H_2, see A. Vigalok, Y. BenDavid, D. Milstein, *Organometallics* **1996**, *15*, 1839–1844; D. M. Heinekey, M. H. Voges, D. M. Barnhart, *J. Am. Chem. Soc.* **1996**, *118*, 10792–10802.

[57] G. J. Kubas, *Metal Dihydrogen and s-Bond Complexes*, Kluwer Academic Publishers, New York, **2001**.

[58] G. J. Kubas, *Catal. Lett.* **2005**, *104*, 79–101.

[59] C. A. Sandoval, T. Ohkuma, K. Muniz, R. Noyori, *J. Am. Chem. Soc.* **2003**, *125*, 13490–13503.

[60] S. E. Clapham, A. Hadzovic, R. H. Morris, *Coord. Chem. Rev.* **2004**, *248*, 2201–2237.

[61] Y. Nishibayashi, I. Takei, M. Hidai, *Angew. Chem.* **1999**, *111*, 3244–3247; *Angew. Chem. Int. Ed.* **1999**, *38*, 3047–3050.

[62] I. Takei, Y. Nishibayashi, Y. Ishii, Y. Mizobe, S. Uemura, M. Hidai, *J. Organomet. Chem.* **2003**, *679*, 32–42.

[63] E. S. Shubina, N. V. Belkova, A. N. Krylov, E. V. Vorontsov, L. M. Epstein, D. G. Gusev, M. Niedermann, H. Berke, *J. Am. Chem. Soc.* **1996**, *118*, 1105–1112.

[64] E. I. Gutsul, N. V. Belkova, M. S. Sverdlov, L. M. Epstein, E. S. Shubina, V. I. Bakhmutov, T. N. Gribanova, R. M. Minyaev, C. Bianchini, M. Peruzzini, F. Zanobini, *Chem. Eur. J.* **2003**, *9*, 2219–2228.

[65] H. S. Chu, C. P. Lau, K. Y. Wong, W. T. Wong, *Organometallics* **1998**, *17*, 2768–2777.

[66] Y. F. Lam, C. Q. Yin, C. H. Yeung, S. M. Ng, G. C. Jia, C. P. Lau, *Organometallics* **2002**, *21*, 1898–1902.

[67] M. Jimenez-Tenorio, M. D. Palacios, M. C. Puerta, P. Valerga, *Organometallics* **2005**, *24*, 3088–3098.

[68] The minimum corresponding to **8** is likely to be owing to the wall potential placed at 0.08 with respect to CN(O). On the other hand, the static DFT approach indicates that complex **8** (Figure 7) is the transition state (see ref. [21]), which confirms the apparent minimum of **8** as an artifact.

[69] The enhancement of the instability of **6** may be caused by the wall potential applied to CN(O), which might hinder the formation of a more stable dihydrogen-bonded complex.

[70] The relative stabilities of the complexes shown in Scheme 2 cannot be compared as a result of some biases in the stabilities introduced by simulation parameters, such as wall potentials. The potential energies obtained by the static methods can be found in ref. [21].

Received: February 13, 2007
Published online: June 13, 2007

